

## Octupole shapes and shape changes at high spins in the $Z \approx 58$ , $N \approx 88$ nuclei

W. Nazarewicz\*

*Department of Physics, Florida State University, Tallahassee, Florida 32306  
and Joint Institute for Heavy Ion Research, Holifield Ion Research Facility, P.O. Box 2008, Oak Ridge, Tennessee 37831*

S. L. Tabor

*Department of Physics, Florida State University, Tallahassee, Florida 32306*

(Received 29 August 1991)

The shapes of rotating Xe, Ba, Ce, Nd, and Sm nuclei ( $84 \leq N \leq 94$ ) are calculated using the cranking model with the Woods-Saxon average potential and pairing. The lightest isotopes of Xe and Ba have nearly spherical ground states, but develop octupole and quadrupole deformations under rotation which remain up to very high spins. The ground states of the heavier isotopes have octupole and quadrupole deformations which persist up to medium spins ( $I \approx 12\hbar$ ). At higher spins, a shape transition is predicted to reflection-symmetric aligned many-quasiparticle configurations.

PACS number(s): 21.10.Ky, 21.10.Re, 21.60.Jz, 27.60.+j

### I. INTRODUCTION

Nuclei with strong octupole correlations have particularly low-lying negative parity states. For vibrational systems those states correspond to one-phonon octupole excitations and for nuclei with stable octupole deformation they represent the members of parity doublets. From the systematics of negative parity excitations one learns that the nuclei with the strongest octupole correlations are the neutron-deficient nuclei around  $^{224}\text{Th}$  (with negative parity excitations of the order of 200 keV) and the neutron-rich nuclei around  $^{146}\text{Ba}$  (with the energy of the lowest  $1^-$  state about 750 keV).

The reason that regions of very strong octupole correlations are fairly well localized around particular proton and neutron numbers can be understood from the structure of the spherical single-particle spectrum. The tendency towards maximal octupole coupling occurs just above the closed shells, i.e., for  $Z$  or  $N \approx 34, 56, 88$ , and 134, where the  $(N, l, j)$  intruder orbitals interact with the  $(N-1, l-3, j-3)$  normal-parity states through the octupole component in the nuclear Hamiltonian. For example, in the nuclei around  $^{146}\text{Ba}$  such pairs of octupole-driving orbitals are the  $\nu i_{13/2}-\nu f_{7/2}$  and  $\pi h_{11/2}-\pi d_{5/2}$  states. Generally, the energy distance between such orbitals decreases with increasing mass number while the number of matrix elements of the octupole interaction increases. This explains why the octupole coupling in the Ra-Th region is stronger than in the Ba-Nd nuclei (see discussion in Ref. [1]).

Low-energy negative parity bands in nuclei around  $^{150}\text{Sm}$  can be most likely associated with the octupole vi-

brational mode [2]. In an early paper based on the random phase approximation approach Neergård and Vogel pointed out [3] that the energy of the  $K^\pi=0^-$  octupole vibrational state decreases when approaching  $Z=62$ ,  $N=90$ . At the same time the octupole strength increases markedly. For  $^{152}\text{Sm}$  the estimated value of dynamic octupole deformation turned out to be as large as  $\beta_3=0.11$ . Similar results were obtained in works by the Dubna group [4]: The  $K^\pi=0^-$  octupole states were predicted to be lower in energy and more collective than the  $K^\pi=1^-$  and  $2^-$  states. The dominant components in the one-phonon  $K^\pi=0^-$  wave function are two-quasiparticle configurations involving the  $\nu i_{13/2}$  or  $\pi h_{11/2}$  unique-parity orbitals which carry a large amount of aligned angular momentum. With increasing rotational frequency they come down in energy and cross the octupole vibrational band. It has thus been concluded [5] that at higher spins the lowest negative parity bands based on collective octupole states must have a two-quasiparticle character. However, when approaching  $Z=56$  and  $N=88$  this simple scenario does not hold. The octupole interaction becomes so strong that it leads to the octupole instability and the lowest negative parity bands have a much more complex structure.

The main objective of this investigation is to stress the importance of shape changes and pairing correlations in the description of quasimolecular rotational bands around  $^{148}\text{Ce}$ . Predictions have been made for those nuclei which show the best prospects of having reflection-asymmetric rotational bands at relatively low excitation energies. Some preliminary results of these calculations were presented in Refs. [6,7]. A summary of reflection-asymmetric mean-field calculations in the  $^{148}\text{Ce}$  region is given in Sec. II. The model is described in Sec. III. The results of the calculations are presented in Sec. IV. In Sec. V a short comment is made on intrinsic dipole moments in the quasimolecular bands. The summary and conclusions are contained in Sec. VI.

\*Permanent address: Institute of Theoretical Physics, Warsaw University, ul. Hoża 69, PL-00-681 Warsaw, Poland.

## II. OCTUPOLE INSTABILITY AROUND $^{148}\text{Ce}$ IN THE MEAN-FIELD APPROACH

The deformed shell model indicates that  $Z=56$  as well as  $N=88$  are the optimal particle numbers for octupole instability [8,1]. Indeed, at these particle numbers a shell structure appears in the single-particle spectrum which strongly favors octupole correlations. The single-particle Woods-Saxon levels for protons and neutrons without rotation are displayed in the left portion of Figs. 1 and 2, respectively, as a function of octupole deformation  $\beta_3$ . Due to octupole mixing between the  $h_{11/2}$  and  $d_{5/2}$  subshells two large energy gaps open up at  $Z=56$  and  $Z=62$  in the proton spectrum. In the neutron system the large gap at  $N=88$  can be seen—as a result of the  $i_{13/2}$ - $f_{7/2}$  octupole interaction. A close inspection of Figs. 1 and 2 leads to the conclusion that at large octupole deformations the single-particle levels become nearly degenerate forming the quasi- $j$  subshells. For example, at  $\beta_3=0.15$  the two orbitals with  $\Omega=\frac{1}{2}$  and  $\frac{3}{2}$  are close to each other just below the  $Z=56$  gap in Fig. 1, forming a “ $j$ ”= $\frac{3}{2}$  multiplet. Similar “ $j$ ”= $\frac{5}{2}$  and “ $j$ ”= $\frac{7}{2}$  multiplets can be seen above the  $Z=56$  and  $Z=62$  gaps, respectively. Analogous structure can also be observed in the neutron system (see Fig. 2).

The general conditions for shell structure have been formulated by Bohr and Mottelson [9]. Large energy closures for any spherical potential can be related to closed quasiclassical trajectories characterized by an integer ratio between the radial and angular oscillations. Octupole shapes can be associated with a 3:1 ratio corresponding to orbits of a triangular type (cf. also discussion in Ref. [8]). The strong shell effects pointed out above arise from this simple 3:1 symmetry.

At spherical shape the strongly octupole interacting subshells, i.e.,  $\nu i_{13/2}$ - $\nu f_{7/2}$  and  $\pi h_{11/2}$ - $\pi d_{5/2}$ , are about 2 MeV apart (see, e.g., Fig. 2 of Ref. [10]). With increasing quadrupole deformation, orbitals belonging to the

unique-parity subshells approach the normal-parity states which have the same  $\Omega$ -quantum number. For unique-parity states both  $j$  and  $l$  are approximately good quantum numbers even at large deformations. This is not true for normal-parity states which are strongly mixed by the quadrupole interaction. Due to this fragmentation the simple two  $j$ -shell picture is no longer valid and as a consequence all the states of opposite parity with the same  $\Omega$  values are coupled by the octupole interaction (assuming the  $K=0$  part of the octupole interaction to be dominant).

As a result of strong shell effects the reflection-asymmetric mean-field theory predicts octupole instability and octupole softness in a number of nuclei from the  $^{146}\text{Ba}$  region. In the Woods-Saxon model calculations of Refs. [1,10,11] a number of lanthanide nuclei were expected to be octupole deformed at their ground states. In all cases considered, the nuclei with octupole-deformed ground states have been calculated to have sizable quadrupole and hexadecapole deformations, as a consequence of the fragmentation mechanism discussed above.

Octupole instability around  $^{146}\text{Ba}$  has also been predicted by the folded-Yukawa model (for comparison with the Woods-Saxon model see Fig. 7 of Ref. [1]) as well as by self-consistent calculations based on Skyrme or Gogny forces [12,13]. All these models yield similar results for octupole deformations, but give slightly different predictions for the height of the octupole barrier (the latter quantity is very sensitive to the energy distance between pairs of states interacting via the octupole force [1]).

In the mass calculations by Möller and Nix [14] based on the folded-Yukawa model the nuclei around  $^{146}\text{Ba}$  were systematically underbound by a few hundred keV. Inclusion of octupole deformation turned out to remove a part of this discrepancy [15]. Another contribution to the binding energy may arise from the zero-point octupole fluctuations, cf. Ref. [8]. Some attempts towards including dynamic corrections by means of parity projec-

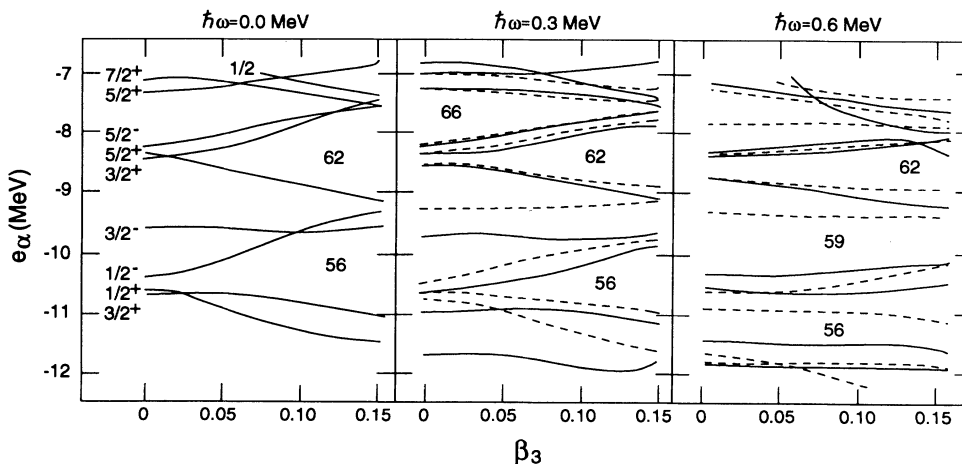


FIG. 1. Single-particle Woods-Saxon levels for protons plotted versus octupole deformation  $\beta_3$  at fixed values of  $\beta_2=0.2$  and  $\beta_4=0.08$ . At zero rotational frequency,  $\hbar\omega=0$ , the single-particle levels are labeled by means of the  $\Omega$  quantum number. The intrinsic parity quantum number,  $\pi$ , is indicated only at  $\beta_3=0$  (for  $\beta_3\neq 0$  the intrinsic parity is violated). At  $\hbar\omega > 0$  the levels are labeled by means of the simplex quantum number:  $s = i$  (solid line) and  $s = -i$  (dashed line).

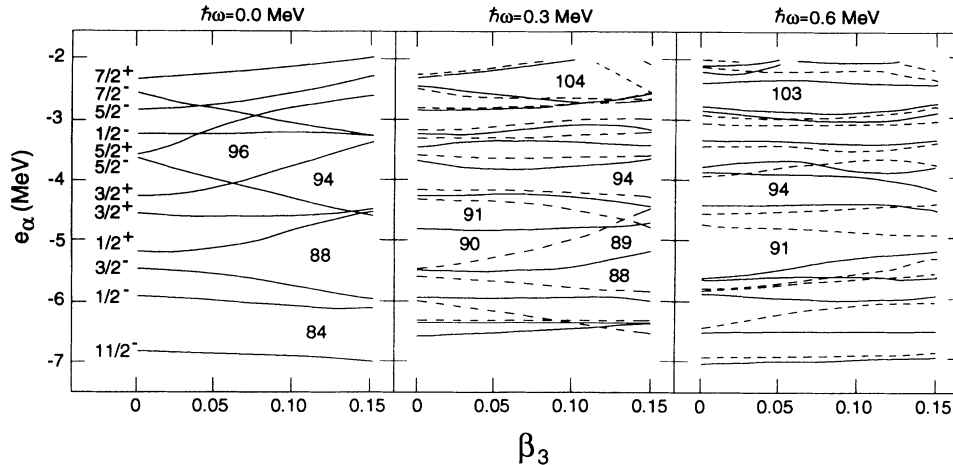


FIG. 2. Similar to Fig. 1 but for neutrons.

tion or the Gaussian overlap approximation have been made in Refs. [12,13]. The first results of those calculations look very encouraging and they will, hopefully, be extended to the domain of high angular momentum.

Within the shell-correction method there are other effects which may lower the octupole minima even more. In recent studies [11,16] it has been pointed out that by treating higher-order multipole deformations ( $\beta_5, \beta_6, \dots$ ) in a self-consistent manner it is possible to increase the octupole barriers in the lanthanides. For instance, by inclusion of higher-order deformations the octupole minima in  $^{144,146,148}\text{Ba}$  are lowered by 200–300 keV as compared to the results of Ref. [1].

### III. THE MODEL

The nuclear mean field is parametrized by a Woods-Saxon single-particle potential and a BCS pair field. The surface deformation parameters  $\beta_i$  and the BCS field parameters  $\Delta_p$  and  $\Delta_n$ , for protons and neutrons, respectively, are treated as variational parameters. Cranking implies that the system is constrained to rotate around a fixed axis (the  $x$  axis) at a given frequency  $\omega$ , which is equivalent to minimizing the Routhian  $H_\omega = H - \omega I_x$ , instead of the Hamiltonian  $H$ , with respect to variations of the mean field. At fixed deformation this is achieved by solving the cranked Hartree-Fock-Bogolyubov (CHFb) equations using a sufficiently large space of Woods-Saxon single-particle states. The solution provides the generalized Bogolyubov transformation from single-particle to rotating quasiparticle states, and the self-consistent values of the pairing gap parameters  $\Delta$ . From this it is straightforward to obtain the angular momentum and the energy relative to the nonrotating state at  $\omega=0$ . The energy of the nonrotating state as a function of deformation is obtained by the Strutinsky method. The total Routhian at frequency  $\omega$  and deformation  $\hat{\beta}$  is thus obtained as

$$E^\omega(\hat{\beta}) = E_{\text{Strut}}(\hat{\beta}) + (\langle H_\beta^\omega \rangle_{\text{CHFb}} - \langle H_\beta^{\omega=0} \rangle_{\text{BCS}}). \quad (3.1)$$

The calculations are carried out on a lattice in deformation space, and the results at fixed  $\omega$  are interpolated be-

tween the lattice points. The absolute minimum of the Routhian at fixed  $\omega$  corresponds to the solution for an yrast state. Secondary minima correspond to other solutions, which may be yrast if they have higher angular momentum.

In the present work we employed essentially the same model, which has been applied to high-spin states of reflection-asymmetric actinide nuclei [17]. The axially deformed Woods-Saxon average potential of Ref. [18] was used with the parameter set of Ref. [19]. In the Strutinsky approach to calculating the energy at  $I=0$ , the level spectrum in the single-particle potential is used to calculate a quantal shell correction. This was done with a smoothing range  $\gamma = 1.2\hbar\omega_0$ , where  $\hbar\omega_0 = 41/A^{1/3}$  MeV, and a correction polynomial of order  $p=6$  (Ref. [20]). For the macroscopic energy we have used the Yukawa-plus-exponential mass formula of Ref. [14]. It takes into account surface diffuseness and finite-range effects, which are significant for higher multipole deformations.

The nuclear shape was defined by the standard  $\beta_\lambda$  parametrization for axial shapes:

$$R(\Omega) = c(\beta)R_0 \left[ 1 + \sum_{\lambda=2}^6 \beta_\lambda Y_{\lambda 0}(\Omega) \right], \quad (3.2)$$

with  $c(\beta)$  being determined from the volume-conservation condition and  $R_0 = r_0 A^{1/3}$ . Only the quadrupole ( $\beta_2$ ), octupole ( $\beta_3$ ), and hexadecapole ( $\beta_4$ ) deformations were treated as variational parameters. The deformation lattice had nine points in the direction of  $\beta_2$ , six points in the direction of  $\beta_3$ , and three points in the direction of  $\beta_4$ . To optimize the calculations the  $\beta_4$  grid was defined relatively to the  $\beta_4(\beta_2, \beta_3)$  average equilibrium deformation trajectory of Ref. [1]. The rotational frequency was varied from  $\hbar\omega=0$  to 0.5 MeV in steps of 0.05 MeV. The calculations cover the region of nuclei with  $54 \leq Z \leq 64$  and  $84 \leq N \leq 94$ .

The higher-order deformations  $\beta_5$  and  $\beta_6$  were taken as the following functions of  $\beta_2, \beta_3$ , and  $\beta_4$ :

$$\begin{aligned}\beta_5 &= \beta_3(0.177\beta_2 + 0.655\beta_4 - 0.0352\beta_3^2 + 0.0089), \\ \beta_6 &= -0.2215\beta_4^2 + 0.1055\beta_3^2 + 0.1476\beta_2\beta_4 - 0.0285\beta_2^3.\end{aligned}\quad (3.3)$$

These expressions minimize the liquid-drop energy [1].

The short-range residual interaction was approximated by a monopole pairing force with the strength,  $G$ , taken according to Ref. [21]. At zero rotational frequency the pairing gap  $\Delta_0$  was determined self-consistently using the BCS method. At high spins, however, the Coriolis force acts destructively on the mean pair field with a corresponding reduction of the static gap parameter. When BCS trial wave functions are used with the CHFB method (rotating BCS, RBCS),  $\Delta$  suddenly drops to zero at a certain value of  $\omega = \omega_{\text{crit}}$ . However, a smoother variation of the pairing energy with  $\omega$  is obtained if the minimization of the total Routhian with respect to  $\Delta$  is carried out after good particle number has been projected from the solution of the CHFB equations. Then the pairing correlations are present to some extent at all frequencies [22]. The particle-number projection method before variation (RFBCS) requires much more computer time than the standard RBCS approach, however, and for the systematic large-scale calculations of the equilibrium deformations we adopted the following simplified procedure.

(i) For a few nuclei at a number of selected deformation points we carried out calculations using the RFBCS method. It turned out that the effective pairing gap defined as

$$\Delta_r \equiv G\sqrt{\langle \hat{P}^\dagger \hat{P} \rangle}, \quad (3.4)$$

where  $\hat{P}^\dagger$  is the pair creation operator, was *on average* reduced by about 50% at  $\hbar\omega_c = 0.55$  and 0.42 MeV for protons and neutrons, respectively.

(ii) At each deformation point we solved the RBCS equations with  $\omega$ -dependent values of  $\Delta$  defined by

$$\Delta(\omega) = \begin{cases} \Delta_0 \left[ 1 - \frac{1}{2} \left( \frac{\omega}{\omega_c} \right)^2 \right] & \text{if } \omega < \omega_c, \\ \frac{1}{2} \Delta_0 \exp \left[ -2 \left( \frac{\omega}{\omega_c} \right) + 2 \right] & \text{if } \omega > \omega_c. \end{cases} \quad (3.5)$$

(iii) The chemical potential  $\lambda$  of the RBCS equations was adjusted at each deformation and rotational frequency separately so as to solve the particle-number equation

$$N = \langle \hat{N} \rangle. \quad (3.6)$$

#### IV. INTERPLAY BETWEEN OCTUPOLE DEFORMATION AND ROTATION

Some of the strongest evidence for stable octupole deformation is the existence of quasimolecular bands consisting of positive and negative parity levels connected by very fast  $E1$  transitions. Such bands are well known in the region of light actinide nuclei around  $^{224}\text{Th}$ . As a typical example, Fig. 3 displays the experimental Routhians,  $E^\omega = E - \omega I_x$ , and the dynamical moments of inertia,  $\mathcal{J}^{(2)} = dI_x/d\omega$ , for  $^{224,226}\text{Th}$  as a function of rotational

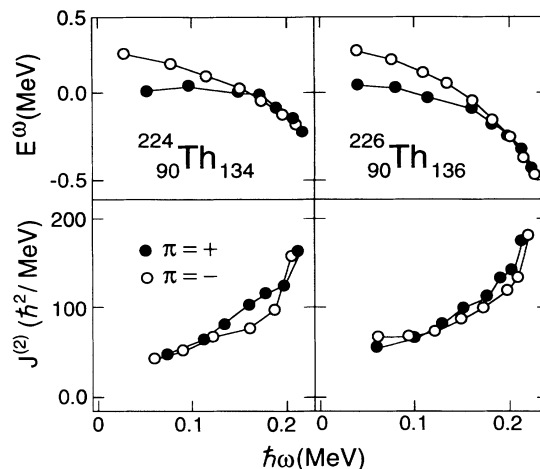


FIG. 3. Experimental Routhians (top) and dynamical moments of inertia (bottom) for the positive (closed circles) and negative (open circles) parity yrast bands in  $^{224,226}\text{Th}$ . The Routhians are plotted with respect to the smooth reference obtained by a Harris expansion of the bottom part of the  $\pi = +$  bands. The experimental data were taken from Ref. [23].

frequency. It is seen that for  $\hbar\omega \gtrsim 150$  keV both  $\pi = +$  and  $\pi = -$  Routhians and moments of inertia merge forming one alternating parity sequence.

In  $^{144}\text{Ba}$  (and probably also in  $^{146}\text{Ba}$ ) (Ref. [24]) the positive and negative parity bands merge at  $\hbar\omega \gtrsim 0.2$  MeV forming a quasimolecular band; see Fig. 4. A similar pattern has also been observed in  $^{144}\text{Ce}$  (Ref. [25]),  $^{146}\text{Ce}$  (Ref. [26]),  $^{146}\text{Nd}$  (Ref. [7]),  $^{148}\text{Nd}$  (Refs. [7,27]),  $^{148}\text{Sm}$  (Refs. [28,29]), and  $^{150}\text{Sm}$  (Ref. [30]), above  $I = 8$ . With increasing proton number the energy displacement between the lowest negative and positive parity bands becomes larger. For example, in  $^{152}\text{Gd}$  the negative parity

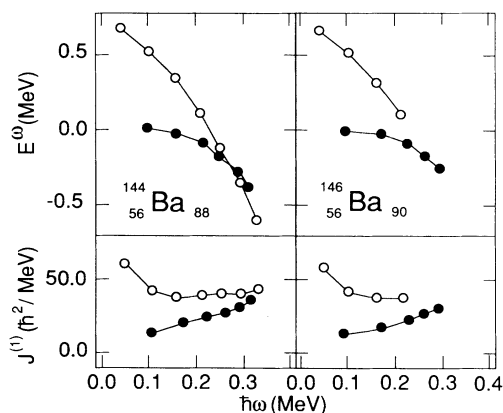


FIG. 4. Experimental Routhians (top) and kinematic moments of inertia,  $\mathcal{J}^{(1)} = I_x/\omega$  (bottom), for the positive (closed circles) and negative (open circles) parity yrast bands in  $^{144,146}\text{Ba}$ . The Routhians are plotted with respect to the smooth reference obtained by a Harris expansion of the bottom part of the  $\pi = +$  bands. The experimental data were taken from Ref. [24].

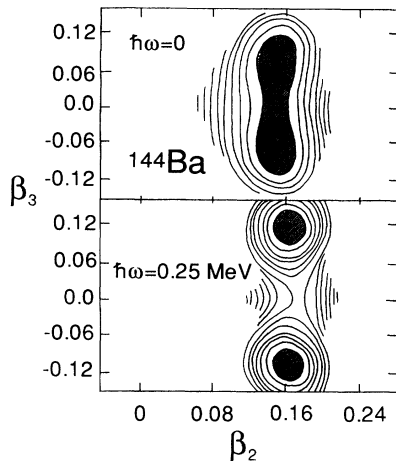


FIG. 5. Total Routhian surface in the  $(\beta_2, \beta_3)$  plane for  $^{144}\text{Ba}$  at  $\hbar\omega=0$  and 0.25 MeV. At each  $(\beta_2, \beta_3)$  point the total Routhian was minimized with respect to hexadecapole deformation  $\beta_4$ . The difference between contour lines is 100 keV.

band lies more than 200 keV above the positive parity yrast band at  $I \approx 11$  (see discussion in Ref. [31]). In odd- $A$  and odd-odd lanthanide nuclei parity doublets have been observed (or suggested) in  $^{149}\text{Sm}$  (Ref. [28]),  $^{151}\text{Pm}$  (Refs. [32–34]),  $^{152}\text{Eu}$  (Ref. [35]),  $^{153,155}\text{Eu}$  (Refs. [32,36]), and  $^{154}\text{Eu}$  (Ref. [37]).

Quasimolecular rotational bands in a reflection-asymmetric nucleus can be characterized by a new quantum number called simplex. The simplex quantum number,  $s$ , is the eigenvalue of the  $PR_x^{-1}$  operator [reflection through the  $(y, z)$  plane] [9] and has properties similar to those of the signature quantum number in the absence of reflection symmetry [38,39]. Octupole coupling between

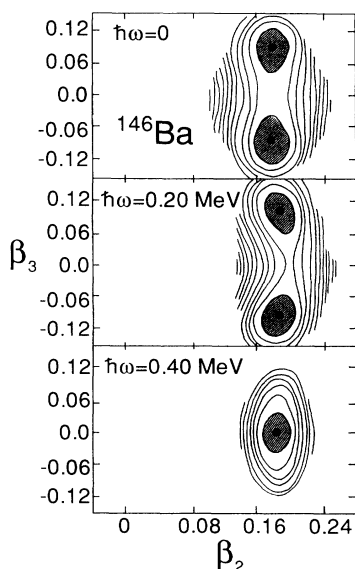


FIG. 6. Similar to Fig. 5 but for  $^{146}\text{Ba}$  at  $\hbar\omega=0$ , 0.20, and 0.40 MeV.

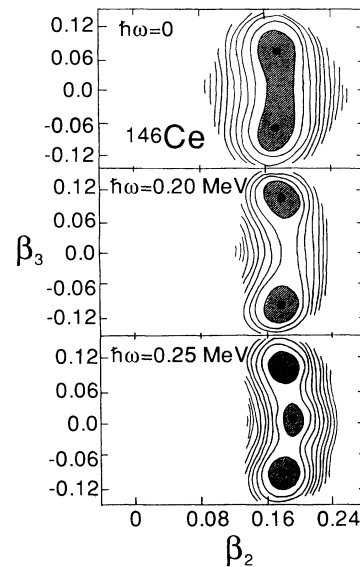


FIG. 7. Similar to Fig. 5 but for  $^{146}\text{Ce}$  at  $\hbar\omega=0$ , 0.20, and 0.25 MeV.

high- $j$  unique-parity orbitals and normal-parity states leads to fragmentation of the aligned angular momentum over many quasiparticle states. The angular momentum content of the lowest Routhians, containing a significant component of high- $j$  unique-parity states, decreases with  $\beta_3$ . On the other hand, the average alignment of Routhians with dominating component of normal parity increases. As a consequence the quasiparticle Routhian pattern becomes more collective, the band-crossing frequency is shifted towards larger values, and the band interaction generally increases (for details see Ref. [39]).

The influence of rotational frequency on the octupole shell structure is shown in Figs. 1 and 2. Single-particle

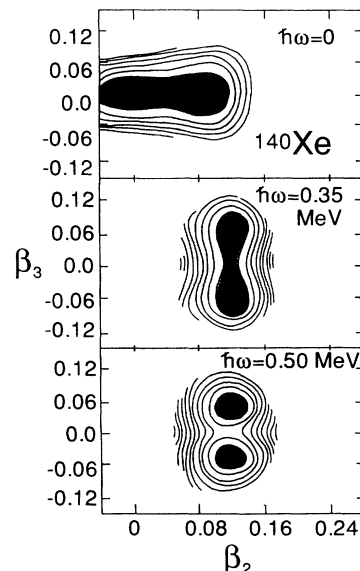


FIG. 8. Similar to Fig. 5 but for  $^{140}\text{Xe}$  at  $\hbar\omega=0$ , 0.35, and 0.50 MeV.

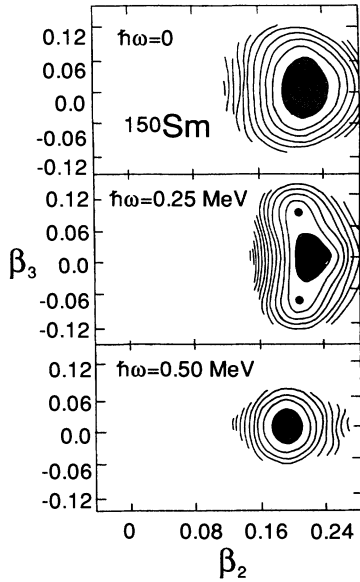


FIG. 9. Similar to Fig. 5 but for  $^{150}\text{Sm}$  at  $\hbar\omega=0$ , 0.25, and 0.50 MeV.

Routhians are plotted vs  $\beta_3$  for two finite values of rotational frequency:  $\hbar\omega=0.3$  and 0.6 MeV. In Fig. 1 at  $\hbar\omega=0.3$  MeV the pattern of single-proton levels is quite similar to that at  $\hbar\omega=0$ : both proton numbers  $Z=56$  and  $Z=62$  are still octupole driving. However, at the higher rotational frequency,  $\hbar\omega=0.6$  MeV, the octupole shell structure is almost completely washed out. An even more dramatic Coriolis-anti-octupole effect is seen in Fig.

2 for the neutrons where the shell effects are already significantly reduced at  $\hbar\omega=0.3$  MeV. This result suggests that at very high spins the octupole shell driving forces are seriously quenched.

In order to understand the enhancement in octupole correlations at medium spins, Woods-Saxon-Bogolyubov cranking calculations were carried out. Selected examples of calculated total Routhian surfaces (TRS) in the  $(\beta_2, \beta_3)$  plane are shown in Figs. 5–9. A summary of the calculated  $(\beta_2, \beta_3)$  equilibrium deformations for the doubly even Xe, Ba, Ce, Nd, Sm, and Gd isotopes is presented in Figs. 10–15. The shape changes in these isotopes follow three different patterns. They are discussed below.

(i)  $^{144}\text{Ba}$  is representative of nuclei with developed quadrupole and octupole deformation in the ground state (see Fig. 5). The calculations indicate that at medium spins the magnitude of octupole deformation increases and the octupole minima are much better separated than in the ground state. The enhancement of octupole strength with rotation is caused [39,17,6] by (a) weaker pairing correlations for the octupole shape, which increase the moments of inertia, and by (b) increased octupole mixing between single-particle states of opposite parity which approach each other with increasing frequency. Other nuclei which show similar behavior are  $^{144}\text{Xe}$ ,  $^{146}\text{Ba}$ , and  $^{144,146}\text{Ce}$ . At frequencies above 0.3 MeV a shape transition towards  $\beta_3=0$  is expected after the alignment of the  $\nu i_{13/2}$  and  $\pi h_{11/2}$  pairs. The strong alignment process that occurs at reflection-symmetric shapes is illustrated in the quasiparticle Routhian diagram of Fig. 16. At  $\hbar\omega > 0.35$  MeV the vacuum configuration at  $\beta_3=0.1$  has a four-quasiparticle struc-

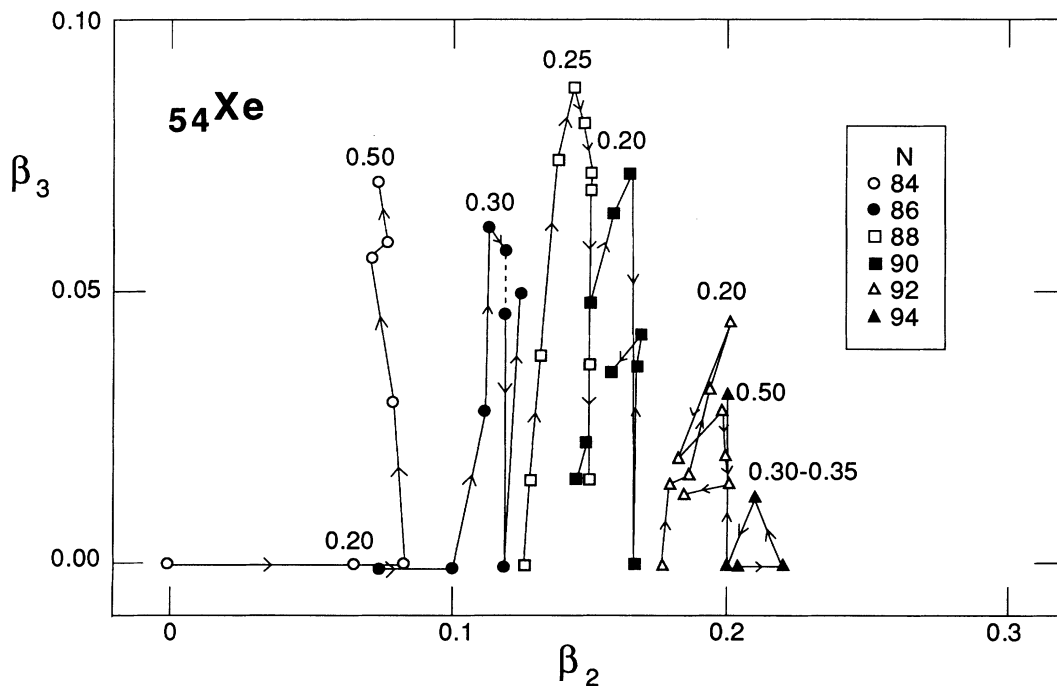


FIG. 10. Calculated equilibrium  $\beta_2, \beta_3$  deformations for the doubly even Xe isotopes with  $84 \leq N \leq 94$  as functions of rotational frequency ( $0 \leq \hbar\omega \leq 0.5$  MeV).

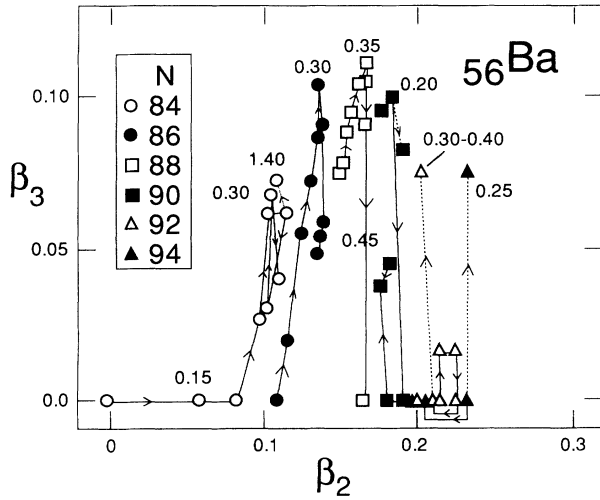


FIG. 11. Similar to Fig. 10 but for the doubly even Ba isotopes. The coexisting excited minima are indicated by dotted lines.

ture (it contains two aligned neutrons and two aligned protons). Since the energy of aligned quasiparticle states is considerably lowered at  $\beta_3=0$ , a shape transition takes place. In the Ra and Th nuclei similar shape changes (caused by the alignment of  $\nu j_{15/2}$  and  $\pi i_{13/2}$  quasiparticles) have also been predicted to occur above  $I=24$  (see detailed discussion in Refs. [39,17]). In the Xe-Sm isotopes the transition to reflection-symmetric shapes is expected to take place around  $I=12$ , which is much easier to reach experimentally. The crossing between reflection-symmetric and reflection-asymmetric configurations is illustrated in Fig. 6 ( $^{146}\text{Ba}$ ) and Fig. 7 ( $^{146}\text{Ce}$ ). The TRS at  $\hbar\omega=0.25$  MeV for  $^{146}\text{Ce}$  shows the coexisting ground band ( $\beta_3 \neq 0$ ) and the aligned configuration ( $\beta_3=0$ ), while only the aligned

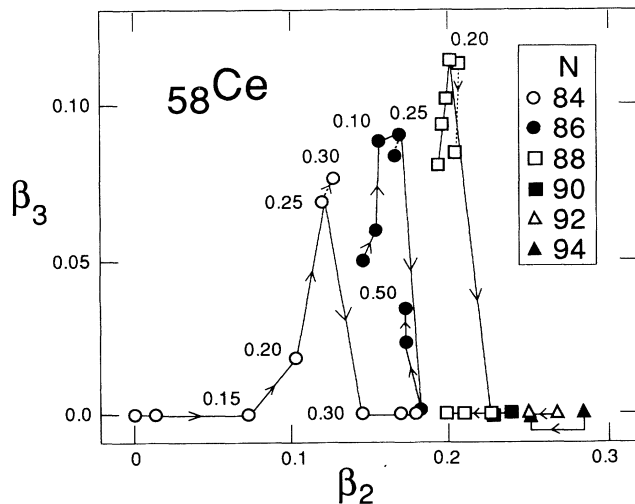


FIG. 12. Similar to Fig. 10 but for the doubly even Ce isotopes. The coexisting excited minima are indicated by dotted lines.

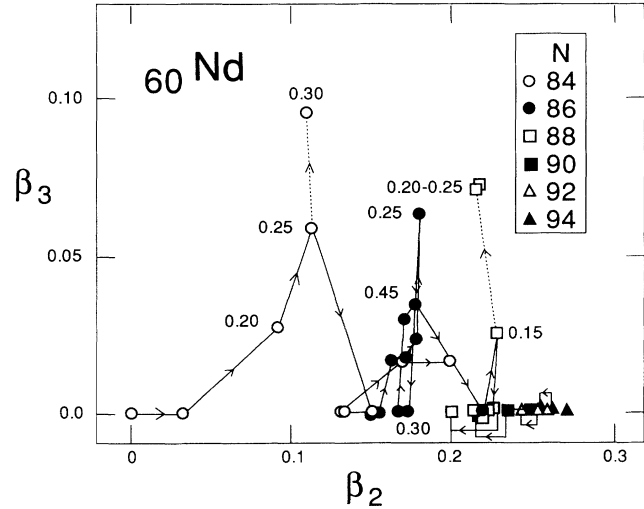


FIG. 13. Similar to Fig. 10 but for the doubly even Nd isotopes. The coexisting excited minima are indicated by dotted lines.

configuration persists at  $\hbar\omega=0.4$  MeV in  $^{146}\text{Ba}$ .

(ii) The nucleus  $^{140}\text{Xe}$  provides an example of strong quadrupole-octupole coupling (see Fig. 8).  $^{140}\text{Xe}$  has a ground-state minimum which is very  $\beta_2$  soft. Since deformed shapes are favored by rotation,  $^{140}\text{Xe}$  becomes octupole deformed at  $\hbar\omega \approx 0.25$  MeV. This shape transition is also associated with an increase in quadrupole deformation. Interestingly, octupole correlations in  $^{140}\text{Xe}$  are calculated to persist up to very high spins. Other nuclei with predicted strong quadrupole-octupole coupling are  $^{138}\text{Xe}$ ,  $^{140,142}\text{Ba}$ ,  $^{142}\text{Ce}$ ,  $^{144}\text{Nd}$ , and  $^{146}\text{Sm}$ .

(iii) This group contains nuclei with well developed quadrupole deformations, and  $\beta_3$ -soft (but reflection-symmetric) shapes in the ground state. At low frequencies the negative parity states in these nuclei can be described in terms of very collective octupole vibrations. However, at medium spins the static theory predicts a shape transition towards  $\beta_3 \neq 0$  or just the presence of

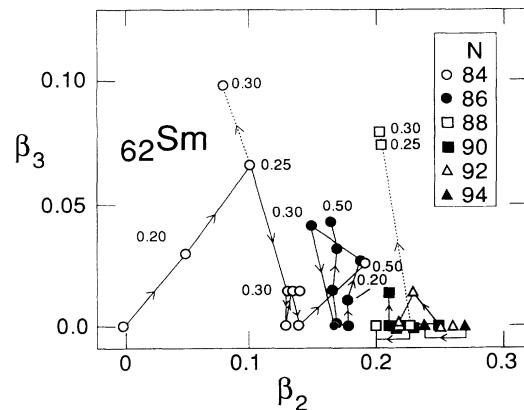


FIG. 14. Similar to Fig. 10 but for the doubly even Sm isotopes. The coexisting excited minima are indicated by dotted lines.

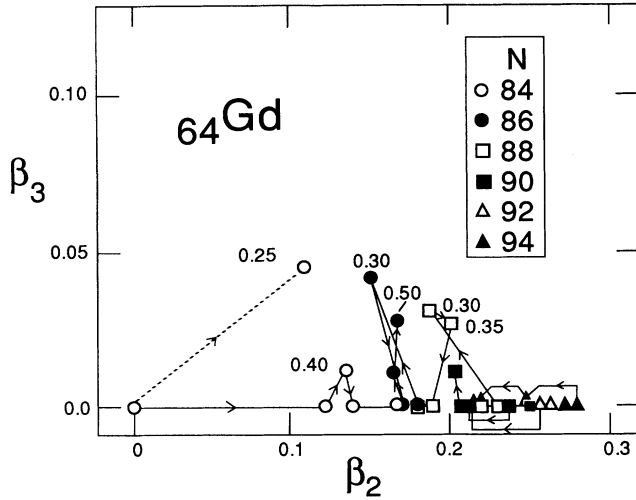


FIG. 15. Similar to Fig. 10 but for the doubly even Gd isotopes. The coexisting excited minima are indicated by dotted lines.

near-yrast reflection-asymmetric configurations. The nuclei that belong to this group are  $^{146}\text{Xe}$ ,  $^{148}\text{Ba}$ ,  $^{146,148}\text{Nd}$ ,  $^{148,150}\text{Sm}$ , and  $^{150,152}\text{Gd}$ . The enhancement of octupole correlations at medium spins in  $^{150}\text{Sm}$  is illustrated in Fig. 9 (for analogous diagrams for  $^{146,148}\text{Nd}$  and  $^{148}\text{Sm}$  we refer the reader to Ref. [7] and Ref. [29], respectively). At the ground state the nucleus  $^{150}\text{Sm}$  is octupole soft but reflection symmetric. At medium spins, however, the octupole-deformed configuration is predicted to become yrast (or close to yrast). After the first quasiparticle crossing only one, reflection-symmetric minimum is seen in the TRS ( $\hbar\omega=0.5$  MeV). The recent experimental data by Urban *et al.* on  $^{146}\text{Nd}$  (Ref. [7]),  $^{148}\text{Sm}$  (Ref. [29]), and  $^{150}\text{Sm}$  (Ref. [30]) indeed suggest that the above scenario takes place in these nuclei. In particular, a band crossing associated with a shape change has been observed.

Since our calculations have been restricted to axial shapes, we cannot describe quantitatively the rotation-induced interplay between triaxial and reflection-asymmetric shapes. For systems, which are  $\gamma$  soft, like  $^{146}\text{Nd}$  or  $^{148}\text{Sm}$ , the angular momentum alignment of high- $j$  quasiparticles induces a change towards triaxial shapes [40]. In the case of the  $Z \approx 60$ ,  $N \approx 88$  nuclei the neutron and proton Fermi levels lie in the vicinity of high- $j$ , low- $\Omega$  Nilsson orbitals, respectively. It is, therefore, very likely that for aligned two-quasiparticle configurations the nuclear shape is strongly triaxial. At still higher spins one can expect terminations of quasiparticle structures at oblate shape and a transition to the noncollective regime, or a coexistence between collective and particle-hole configurations. The coupling between  $\gamma$  and  $\beta_3$  deformations in the ground state of  $^{148}\text{Sm}$  has been recently discussed by Skalski [41]. He demonstrated that the corresponding potential energy surface is very shallow in both directions, which suggests a possible transition to the triaxial-octupole regime, or to the noncollective limit at high spins. The above theoretical indications

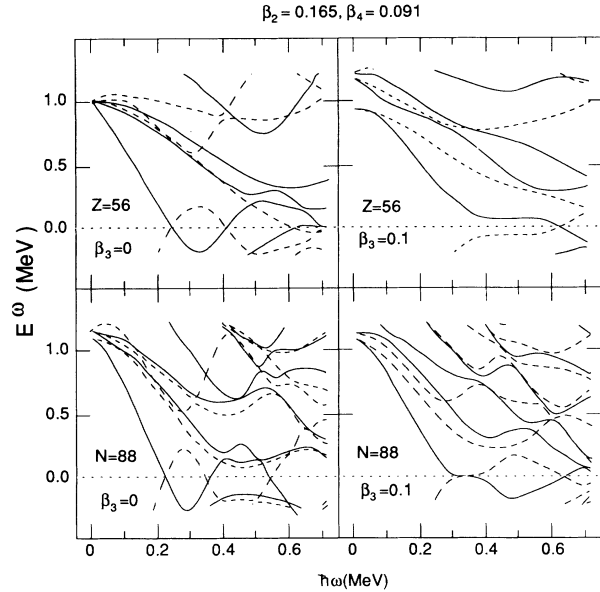


FIG. 16. Proton quasiparticle Routhians for  $Z=56$  (top) and neutron quasiparticle Routhians for  $N=88$  (bottom) as function of rotational frequency. The deformation parameters used correspond to the yrast configurations of  $^{144}\text{Ba}$ . The left panel,  $\beta_3=0$ , is representative of the reflection-symmetric configurations involving aligned neutron and proton pairs. The right panel,  $\beta_3=0.1$ , represent the structure of quasiparticle excitations associated with the reflection-asymmetric ground band. Levels are labeled by means of the simplex quantum number:  $s=i$  (solid line) and  $s=-i$  (dashed line).

are supported by experimental data, which show characteristic quasiparticle excitations in both  $^{146}\text{Nd}$  and  $^{148}\text{Sm}$  (Ref. [29]). They can be nicely compared to well-known shell-model configurations in heavier  $N=86$  isotones.

## V. $E1$ AND $E3$ TRANSITIONS

If the nuclear mean field is not reflection symmetric (e.g., due to octupole deformation) a large  $E1$  moment may arise in the intrinsic frame of a nucleus. Such a dipole moment should manifest itself by very enhanced  $E1$  transitions between opposite parity members of quasi-molecular bands.

The shell-correction approach to the isovector dipole moment for octupole-unstable systems has been formulated by Leander [42]. Within this theory the intrinsic dipole moment can be written as

$$D_1 = D_1^{LD} + D_1^{\text{shell}}, \quad (5.1)$$

where  $D_1^{LD}$  is a macroscopic term and  $D_1^{\text{shell}}$  is a shell-correction contribution. The latter term is given by

$$D_1^{\text{shell}} = e(1 + \chi) \left[ \frac{N}{A} \langle z \rangle_p - \frac{Z}{A} \langle z \rangle_n \right], \quad (5.2)$$

where  $\chi$  is the  $E1$  polarizability coefficient and  $\langle z \rangle$  is the Strutinsky renormalized displacement of the center of mass. The quantity  $\langle z \rangle$  shows a smooth oscillatory be-

havior as a function of particle number with the period of oscillation being one oscillator shell [43,6,44]. As discussed in Ref. [44] oscillations in  $\langle z \rangle$  reflect the strength of unique-parity orbitals fragmented by the octupole interaction. The maximum, corresponding to the positive value of  $\langle z \rangle$ , is reached around the middle of the shell. The minimum in  $\langle z \rangle$  occurs just above the shell closure where  $\langle z \rangle$  is negative. In the region around  $^{146}\text{Ba}$  the proton displacement of the center of mass is maximal at  $Z \approx 64$ . The neutron displacement increases smoothly from  $N=82$  (minimum) to  $N=104$  (maximum).

The isotonic variation of  $D_1^{\text{shell}}$  for the Xe-Gd isotopes with  $84 \leq N \leq 94$  is shown in Fig. 17 for two values of rotational frequency:  $\hbar\omega=0$  and  $\hbar\omega=0.35$  MeV. The behavior of  $D_1^{\text{shell}}$  with particle number reflects the oscillations in  $\langle z \rangle$ . Indeed, for a given isotone chain  $D_1^{\text{shell}}$  increases towards  $Z=64$ . On the other hand, for a given isotope sequence the single-particle contribution to the dipole moment decreases with  $N$ —in agreement with Eq. (5.2) (the effective charge for neutrons is negative). This trend depends rather weakly on rotational frequency.

The shell-correction approach to the intrinsic dipole moment, based on calculated equilibrium deformations from the present study, has been applied to the lanthanides in Refs. [6,44] and has provided an overall agreement with the experimental data. It has been shown that in the lanthanides the  $D_1^{\text{LD}}$  contribution is very small due to the cancellation between the charge redistribution and neutron skin terms [44]. Consequently, the total dipole moment is, in a very good approximation, given by  $D_1^{\text{shell}}$ . Interestingly, the Ba isotopes which are predicted to have the largest octupole deformations have considerably reduced dipole moments. In the octupole-soft Nd and Sm isotopes the predicted dipole moments are large because proton and neutron contributions add coherently. In particular, the isotonic and isotopic behavior of  $D_1^{\text{shell}}$  reproduces [45,44] a dramatic quenching of  $E1$  strength observed in  $^{146}\text{Ba}$ . Indeed for the nucleus  $^{146}\text{Ba}$  the calculated value of  $D_1^{\text{shell}}$  is around  $0.02 e \text{ fm}$ , i.e., it is

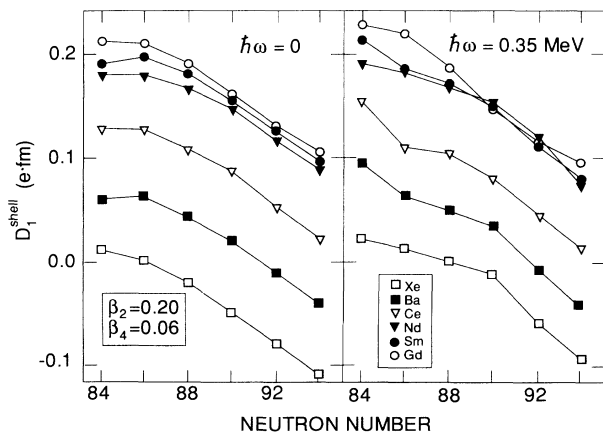


FIG. 17. Isotonic dependence of the shell correction to the intrinsic dipole moment for the Xe-Gd isotopes at  $\hbar\omega=0$  (left) and  $\hbar\omega=0.35$  MeV (right). The average trend does not depend on the actual deformation used (here  $\beta_2=0.2$ ,  $\beta_3=0.06$ ).

about one order of magnitude smaller than that for the isotopes of Nd and Sm ( $D_1^{\text{shell}} \approx 0.2 e \text{ fm}$ ). It has been demonstrated in Ref. [45] that the cancellation of  $D_1$  in  $^{146}\text{Ba}$  is not a local effect, but occurs for a wide range of deformation parameters. This result strongly suggests that even after taking into account dynamic correlations, the very low dipole moment in  $^{146}\text{Ba}$  should remain unchanged [13].

The weak  $\omega$  dependence of  $D_1^{\text{shell}}$  constitutes a microscopic justification for the approximations used in Ref. [44], where it was assumed that rotation enters intrinsic dipole moments only through calculated equilibrium deformations.

The results of recent Coulomb excitation measurements for  $^{148}\text{Nd}$  indicate [46,47] that the average  $\langle \beta_3^2 \rangle$  values extracted from the measured  $E3$  reduced matrix elements stay surprisingly constant as a function of angular momentum. On the other hand, the energy splitting between the positive and negative parity yrast bands quickly decreases with spin; cf. Fig. 3. The latter effect has been attributed, see Sec. IV, to the enhancement of octupole correlations at medium spins. However, since the  $B(E3)$  rates are believed to be a direct measure of octupole collectivity, the experimental results [46] seem to suggest that the octupole correlations in  $^{148}\text{Nd}$  do not show significant angular momentum dependence.

In order to discuss this apparent contradiction we employed the simple collective model for octupole deformation developed by Krappe and Wille [48]. The collective model Hamiltonian is approximated by

$$H = -\frac{\hbar^2}{2D} \frac{d^2}{d\beta_3^2} + V_0 \left[ 1 - \left( \frac{\beta_3}{\bar{\beta}_3} \right)^2 \right]^2, \quad (5.3)$$

where  $D$  is the octupole mass parameter and  $\bar{\beta}_3$  stands for the equilibrium octupole deformation (note that  $\lim_{\bar{\beta}_3 \rightarrow 0} V_0/\bar{\beta}_3^4 = \text{const}$ ). The lowest eigenstates of the Hamiltonian (5.3) with parity  $p = \pm 1$ ,  $\Psi_p$ , can be well approximated by a sum of two Gaussians centered at  $\beta_3 = \pm \bar{\beta}_3$ , i.e.,

$$\Psi_{p=\pm} = \mathcal{N}_{\pm} (\phi \pm \hat{p} \phi), \quad (5.4)$$

where  $\hat{p}$  is the parity operator [ $\hat{p} \phi(\beta_3) = \phi(-\beta_3)$ ] and

$$\phi(\beta_3) = \left( \frac{\lambda}{\pi} \right)^{1/4} \exp \left[ -\frac{\lambda}{2} (\beta_3 - \bar{\beta}_3)^2 \right]. \quad (5.5)$$

The quantity  $\lambda$  in Eq. (5.5) is inversely proportional to the deformation spread of  $\phi$  and is assumed to be the variational parameter of the model [48]. The normalization constants  $\mathcal{N}_{\pm}$  in Eq. (5.4) can be expressed in terms of  $\lambda$  and  $\bar{\beta}_3$  as

$$\mathcal{N}_{\pm} = [2(1 \pm W)]^{-1/2}, \quad W = \langle \phi | \hat{p} | \phi \rangle = \exp(-\lambda \bar{\beta}_3^2). \quad (5.6)$$

The energy difference  $\Delta E = E_- - E_+$  between the lowest  $p = -$  and  $p = +$  states of the Hamiltonian (5.3)

$$E_{\pm} = \langle \Psi_{\pm} | H | \Psi_{\pm} \rangle = \frac{1}{1 \pm W} (\langle \phi | H | \phi \rangle \pm \langle \phi | H | \hat{p} \phi \rangle) \quad (5.7)$$

gives the parity splitting. In order to obtain the variational solution, the ground-state energy,  $E_+$ , has been minimized with respect to  $\lambda$  at a fixed value of  $D$ ,  $V_0$ , and  $\bar{\beta}_3$ .

Figure 18 presents the behavior of  $\Delta E$  as a function of  $V_0$  (the value of  $D$  has been adjusted to reproduce the experimental parity splitting in  $^{144}\text{Ba}$  at calculated values of  $V_0$  and  $\bar{\beta}_3$  at  $I=0$ ). In the same figure, the ratio between the calculated  $B(E3)$  value,

$$B(E3) \propto |\langle \Psi_+ | \beta_3 | \Psi_- \rangle|^2 \propto \frac{\bar{\beta}_3^2}{1 - W^2}, \quad (5.8)$$

and the asymptotic value ( $V_0 \rightarrow \infty$ ) is also shown. The conclusion drawn from Fig. 18 is that the  $B(E3)$  rates depend mainly on the value of equilibrium deformation  $\bar{\beta}_3$  and they are rather insensitive to  $V_0$ . On the other hand, the parity splitting shows significant dependence on  $V_0$ . This result can probably explain, at least qualitatively, the recent data on  $^{148}\text{Nd}$ . At the lowest spins the potential energy surface of  $^{148}\text{Nd}$  is very octupole soft, see [11,16], but at medium spins the reflection-asymmetric configuration is favored by rotation and the octupole barrier increases. Consequently, the  $B(E3)$  values should be influenced by rotation to a much lesser degree than the parity splitting; cf. also results of two-dimensional ( $\beta_2 - \beta_3$ ) calculations of Ref. [49].

Another important mechanism that can influence the parity splitting and  $B(E3)$  values is the effect of the Coriolis and centrifugal forces, i.e., the coupling to higher-lying octupole states with  $K > 0$ . The influence of Coriolis coupling on the moments of inertia of rotational bands built upon the octupole vibrational states has been known for a long time; see, e.g., Refs. [3,9]. In the context of octupole deformations this effect has been discussed recently by Rohoziński *et al.* [50,2], who concluded that  $B(E3)$  is rather insensitive to Coriolis coupling at relatively small values of  $\bar{\beta}_3$  [at large  $\bar{\beta}_3$ 's the perturbed  $B(E3)$  values are actually lower than the unperturbed ones] while the effect on the moment of inertia is tremendous, i.e., the perturbed moment of inertia in the negative parity band is about twice as large as the moment of inertia for the positive parity band, for a rather wide range of  $\beta_3$  values. Consequently, the mechanism in terms of

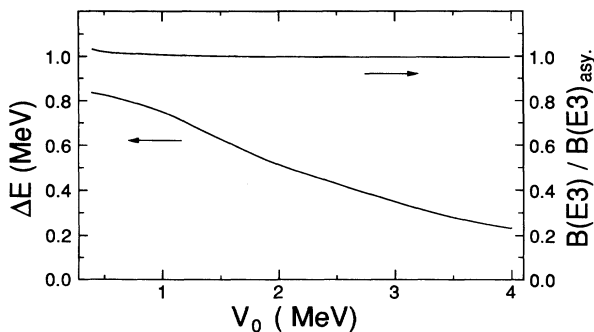


FIG. 18. Parity splitting  $\Delta E$  (left) and the  $B(E3)/B(E3)_{V_0 \rightarrow \infty}$  ratio (right) of a simple collective model of Sec. V as a function of  $V_0$ . For more explanations see text.

strong Coriolis and centrifugal effects would also be consistent with the data for  $^{148}\text{Nd}$ —even without invoking a significant octupole deformation.

## VI. CONCLUSIONS

The present investigation has been focused on the microscopic structure of static octupole correlations at high spin in the  $Z \approx 58$ ,  $N \approx 88$  region. The model used contains the three main building blocks that are governing the properties of near-yrast configurations, i.e., deformation, rotation, and pairing. In spite of its simplicity the deformed shell model turned out to give a fairly good understanding of the angular momentum process in the observed rotational bands. In addition, detailed predictions have been made about the nature and properties of yet unobserved structures. The most important observations made in this paper can be summarized as follows: (i) Static octupole correlations are enhanced at medium spins due to larger moments of inertia at octupole shape caused by weaker pairing correlations and octupole mixing between unique-parity and normal-parity orbitals. (ii) In the lanthanides the shape transition along the yrast line towards  $\beta_3=0$  is expected in the spin region  $I=12$ , i.e., just after the first band crossing. A spectacular example of the coexistence between reflection-symmetric and reflection-asymmetric band structures is  $^{150}\text{Sm}$  (Ref. [30]). (iii) In the  $Z \sim 58$ ,  $N \sim 88$  region the very promising examples of octupole collectivity are the neutron-rich Xe isotopes. In particular, one of the best cases is  $^{144}\text{Xe}$  ( $T_{1/2}=1.2$  s) which is expected to be octupole unstable already at the ground state with, however, a very reduced  $E1$  moment. (iv) The Woods-Saxon-Bogolyubov cranking calculations confirm previous expectations of octupole-deformed mean fields at low and medium spins in the Xe-Sm isotopes with neutron numbers  $84 \leq N \leq 92$ . The best candidates predicted to have octupole-unstable shapes are all Xe, Ba, Ce, Nd, and Sm nuclei with neutron numbers  $N=84, 86, 88$ , and  $^{146}\text{Ba}$  ( $N=90$ ). (v) The largest octupole deformations have been predicted for the Ba and Ce isotopes which, due to shell effects, have considerably reduced dipole moments. On the other hand, in the Nd and Sm isotopes the  $E1$  rates are very strong but these nuclei are apparently less octupole deformed. Consequently, in the nuclei around  $^{146}\text{Ba}$  the quasimolecular bands are not as pronounced as in the Ra-Th nuclei. (vi) The calculated intrinsic dipole moments depend rather weakly on rotational frequency. The main contribution to variations in  $D_1$  with angular momentum comes from deformation changes. (vii) The  $B(E3)$  rates depend mainly on the equilibrium octupole deformation. They are less sensitive to the height of the octupole barrier. The constancy of  $B(E3)$  values with spin, as suggested by the recent data on  $^{148}\text{Nd}$ , does not contradict the predicted enhancement of octupole collectivity at medium spins. However, a similar effect can result from Coriolis and centrifugal coupling to the higher-lying octupole states with  $K > 0$ .

Finally, many properties of the low-energy collective  $E1$  and  $E3$  modes in the transitional nuclei around  $^{146}\text{Ba}$  can be explained by the reflection-asymmetric cranked

mean-field theory. There are also many questions which remain to be answered and more detailed calculations will be necessary. As mentioned already in Sec. II, the self-consistent treatment of fluctuations and higher-order multipole deformations (especially  $\beta_5$ , see Ref. [16]) has to be done when aiming at a quantitative reproduction of experimental data. Also in our discussion the effects of nonaxial deformations have not been taken into account. The lowest band crossing in the lanthanide nuclei discussed is, according to the calculations, associated with the alignment of  $i_{13/2}$  neutrons. The aligned pair of  $i_{13/2}$  quasiparticles is expected to polarize the core towards slightly positive values of  $\gamma$  leading to a sizable nonaxial component in the average field. Another indication of strong gamma effects is the spectrum of  $^{148}\text{Sm}$  (Ref. [29]). The quasimolecular structure, which dominates at medi-

um spins, suddenly terminates above  $I=15$  and the irregular excitation pattern characteristic of noncollective rotation is seen. It suggests a shape transition from an octupole-deformed prolate shape to an oblate noncollective structure with strong octupole correlations.

#### ACKNOWLEDGMENTS

This project was supported in part by the National Science Foundation through Contract No. PHY-89 10648. The Joint Institute for Heavy Ion Research has as member institutions the University of Tennessee, Vanderbilt University, and the Oak Ridge National Laboratory; it is supported by the members and by the Department of Energy through Contract No. DE-FG05-87ER40361 with the University of Tennessee.

- 
- [1] W. Nazarewicz, P. Olanders, I. Ragnarsson, J. Dudek, G. A. Leander, P. Möller, and E. Ruchowska, Nucl. Phys. **A429**, 269 (1984).
- [2] S. G. Rohoziński, Rep. Prog. Phys. **51**, 541 (1988).
- [3] K. Neergård and P. Vogel, Nucl. Phys. **A145**, 33 (1970).
- [4] V. H. Soloviov, *Theory of Complex Nuclei* (Nauka, Moscow, 1971); *Structure of Doubly Even Deformed Nuclei* (Nauka, Moscow, 1974).
- [5] P. Vogel, Phys. Lett. **60B**, 431 (1976).
- [6] W. Nazarewicz, in *Proceedings of the International Conference on Nuclear Structure Through Static and Dynamic Moments*, edited by H. H. Bolotin (Conference Proceedings Press, Melbourne, 1987), p. 180.
- [7] W. Urban, R. M. Lieder, W. Gast, G. Hebbinghaus, A. Krämer-Flecken, T. Morek, T. Rząca-Urban, W. Nazarewicz, and S. L. Tabor, Phys. Lett. B **200**, 424 (1988).
- [8] G. A. Leander, R. K. Sheline, P. Möller, P. Olanders, I. Ragnarsson, and A. J. Sierk, Nucl. Phys. **A388**, 452 (1982).
- [9] A. Bohr and B. R. Mottelson, *Nuclear Structure* (Benjamin, New York, 1975), Vol. 2.
- [10] G. A. Leander, W. Nazarewicz, P. Olanders, I. Ragnarsson, and J. Dudek, Phys. Lett. **152B**, 284 (1985).
- [11] A. Sobiczewski, Z. Patyk, S. Ćwiok, and P. Rozmej, Nucl. Phys. **A485**, 16 (1988).
- [12] P. Bonche, in *The Variety of Nuclear Shapes*, edited by J. D. Garrett *et al.* (World Scientific, Singapore, 1988), p. 302.
- [13] J. L. Egido and L. M. Robledo, Nucl. Phys. **A518**, 475 (1990).
- [14] P. Möller and J. R. Nix, Nucl. Phys. **A361**, 117 (1981).
- [15] P. Möller, W. D. Myers, W. J. Swiatecki, and J. Treiner, At. Data Nucl. Data Tables **39**, 225 (1988).
- [16] S. Ćwiok and W. Nazarewicz, Nucl. Phys. **A496**, 367 (1989).
- [17] W. Nazarewicz, G. A. Leander, and J. Dudek, Nucl. Phys. **A467**, 437 (1987).
- [18] S. Ćwiok, J. Dudek, W. Nazarewicz, J. Skalski, and T. Werner, Comput. Phys. Commun. **46**, 379 (1987).
- [19] J. Dudek, Z. Szymański, and T. Werner, Phys. Rev. C **23**, 920 (1981).
- [20] M. Brack, J. Damgård, A. S. Jensen, H. C. Pauli, V. M. Strutinsky, and C. Y. Wong, Rev. Mod. Phys. **44**, 320 (1972).
- [21] J. Dudek, A. Majhofer, and J. Skalski, J. Phys. G **6**, 447 (1980).
- [22] P. Ring and P. Schuck, *The Nuclear Many-Body Problem* (Springer-Verlag, New York, 1980).
- [23] P. Schüler, Ch. Lauterbach, Y. K. Agarwal, J. de Boer, K. P. Blume, P. A. Butler, K. Euler, Ch. Fleischmann, C. Günther, E. Hauber, H. J. Maier, M. Marten-Tölle, Ch. Schandera, R. S. Simon, R. Tölle, and P. Zeyen, Phys. Lett. B **174**, 241 (1986).
- [24] W. R. Phillips, I. Ahmad, H. Emling, R. Holzmann, R. V. F. Janssens, T.-L. Khoo, and M. W. Drigert, Phys. Rev. Lett. **57**, 3256 (1986).
- [25] A. S. Mowbray, J. B. Fitzgerald, J. L. Durell, M. A. C. Hotchkis, W. R. Phillips, and B. J. Varley, Daresbury Laboratory Annual Report 1988–89, pp. 22–23.
- [26] W. R. Phillips, R. V. F. Janssens, I. Ahmad, H. Emling, R. Holzmann, T.-L. Khoo, and M. W. Drigert, Phys. Lett. B **212**, 402 (1988).
- [27] R. Ibbotson, B. Kotliński, D. Cline, K. G. Helmer, A. E. Kavka, A. Renalds, E. G. Vogt, P. A. Butler, C. A. White, R. Wadsworth, and D. L. Watson, Nucl. Phys. **A530**, 199 (1991).
- [28] E. Hammarén, E. Liukkonen, M. Piiparinen, J. Kownacki, Z. Sujkowski, Th. Lindblad, and H. Ryde, Nucl. Phys. **A321**, 71 (1979).
- [29] W. Urban, R. M. Lieder, J. C. Bacelar, P. P. Singh, D. Alber, D. Balabanski, W. Gast, H. Grawe, G. Hebbinghaus, J. R. Jongman, T. Morek, R. F. Noorman, T. Rząca-Urban, H. Schnare, M. Thoms, O. Zell, and W. Nazarewicz, Phys. Lett. B **258**, 293 (1991).
- [30] W. Urban, R. M. Lieder, W. Gast, G. Hebbinghaus, A. Krämer-Flecken, K. P. Blume, and H. Hübel, Phys. Lett. B **185**, 331 (1987).
- [31] R. K. Sheline and P. C. Sood, Phys. Rev. C **34**, 2362 (1986).
- [32] P. C. Sood and R. K. Sheline, Phys. Rev. C **40**, 1530 (1989).
- [33] W. Urban, J. C. Bacelar, W. Gast, G. Hebbinghaus, A. Krämer-Flecken, R. M. Lieder, T. Morek, and T. Rząca-Urban, Phys. Lett. B **247**, 238 (1990).
- [34] W. J. Vermeer, M. K. Khan, A. S. Mowbray, J. B. Fitzgerald, J. A. Cizewski, B. J. Varley, J. L. Durell, and W. K. Phillips, Phys. Rev. C **42**, R1183 (1990).

- [35] R. K. Sheline and P. C. Sood, *Prog. Theor. Phys.* **81**, 1057 (1989).
- [36] R. K. Sheline and P. C. Sood, *Int. J. Mod. Phys. A* **5**, 2677 (1990).
- [37] R. K. Sheline, *Phys. Lett. B* **219**, 222 (1989).
- [38] W. Nazarewicz, P. Olanders, I. Ragnarsson, J. Dudek, and G. A. Leander, *Phys. Rev. Lett.* **52**, 1272 (1984); **53**, 2060 (1984).
- [39] W. Nazarewicz and P. Olanders, *Nucl. Phys.* **A441**, 420 (1985).
- [40] S. Frauendorf and F. R. May, *Phys. Lett.* **125B**, 245 (1983).
- [41] J. Skalski, *Phys. Rev. C* **43**, 140 (1991); private communication.
- [42] G. A. Leander, in *Capture Gamma-Ray Spectroscopy and Related Topics (Holiday Inn-World's Fair, Knoxville, Tennessee)*, Proceedings of the Fifth International Symposium on Capture Gamma-Ray Spectroscopy and Related Topics, edited by S. Raman, AIP Conf. Proc. No. 125 (AIP, New York, 1984), p. 125.
- [43] G. A. Leander, W. Nazarewicz, G. F. Bertsch, and J. Dudek, *Nucl. Phys.* **A453**, 58 (1986).
- [44] P. Butler and W. Nazarewicz, *Nucl. Phys.* **A533**, 249 (1991).
- [45] H. Mach, W. Nazarewicz, D. Kusnezov, M. Moszyński, B. Fogelberg, L. Spanier, M. Hellström, R. L. Gill, R. F. Casten, and A. Wolf, *Phys. Rev. C* **41**, R2469 (1990).
- [46] C. A. White *et al.*, Liverpool-Rochester-Warsaw Collaboration.
- [47] P. Butler, Proceedings of the International Conference on Nuclear Shapes and Nuclear Structure at Low Excitation Energies, Cargèse, France, 1991 (in press).
- [48] H. J. Krappe and U. Wille, *Nucl. Phys.* **A124**, 641 (1969).
- [49] A. Sobiczewski and K. Böning, *Acta Phys. Pol. B* **18**, 393 (1987).
- [50] S. G. Rohoziński and W. Greiner, *Phys. Lett.* **128B**, 1 (1983).

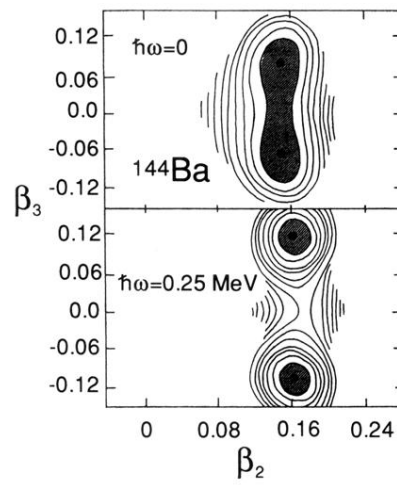


FIG. 5. Total Routhian surface in the  $(\beta_2, \beta_3)$  plane for  $^{144}\text{Ba}$  at  $\hbar\omega=0$  and 0.25 MeV. At each  $(\beta_2, \beta_3)$  point the total Routhian was minimized with respect to hexadecapole deformation  $\beta_4$ . The difference between contour lines is 100 keV.

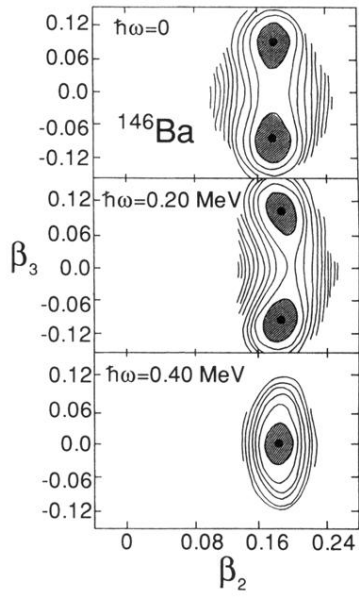


FIG. 6. Similar to Fig. 5 but for  $^{146}\text{Ba}$  at  $\hbar\omega=0, 0.20$ , and  $0.40 \text{ MeV}$ .

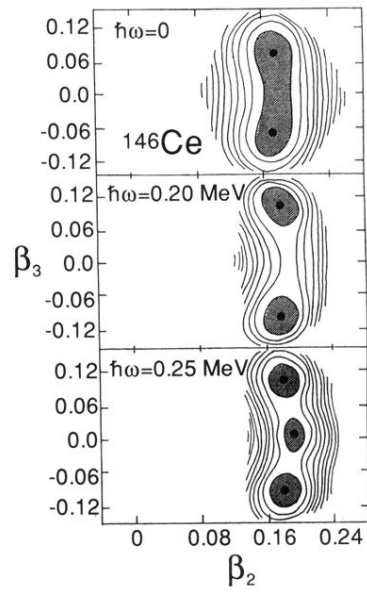


FIG. 7. Similar to Fig. 5 but for  $^{146}\text{Ce}$  at  $\hbar\omega=0$ , 0.20, and 0.25 MeV.

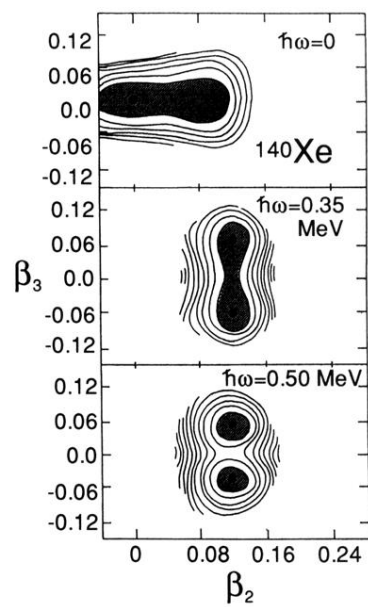


FIG. 8. Similar to Fig. 5 but for  $^{140}\text{Xe}$  at  $\hbar\omega=0$ , 0.35, and 0.50 MeV.

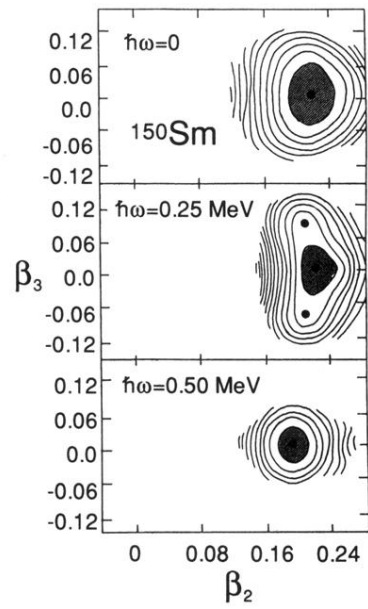


FIG. 9. Similar to Fig. 5 but for  $^{150}\text{Sm}$  at  $\hbar\omega=0$ , 0.25, and 0.50 MeV.